AGU PUBLICATIONS

Geochemistry, Geophysics, Geosystems

RESEARCH ARTICLE
10.1002/2014GC005655

Key Points:
- Sortable-silt "mean size" is not identical with sortable-silt "mean grain size"
- The former may introduce a random element into paleo-current reconstructions
- Differential-number-based statistics may be better suited for paleo-flow studies

Correspondence to:
A. D. Tegzes,
andreategzes@hotmail.com

Citation:
Tegzes, A. D., E. Jansen, and R. J. Telford (2015), Which is the better proxy for paleo-current strength: Sortable-silt mean size ($\overline{SS}$) or sortable-silt mean grain diameter ($\bar{d}_{SS}$)? A case study from the Nordic Seas, *Geochem. Geophys. Geosyst.*, *16*, 3456–3471, doi:10.1002/2014GC005655.

Received 12 NOV 2014
Accepted 11 SEP 2015
Accepted article online 16 SEP 2015
Published online 17 OCT 2015

Which is the better proxy for paleo-current strength: Sortable-silt mean size ($\overline{SS}$) or sortable-silt mean grain diameter ($\bar{d}_{SS}$)? A case study from the Nordic Seas

Andrea D. Tegzes[1], Eystein Jansen[2], and Richard J. Telford[3]

[1]UNI Research and Bjerknes Centre for Climate Research, Bergen, Norway, [2]Department of Earth Science and Bjerknes Centre for Climate Research, University of Bergen, Bergen, Norway, [3]Department of Biology and Bjerknes Centre for Climate Research, University of Bergen, Bergen, Norway

Abstract The coarseness of the 10–63 μm terrigenous silt (i.e., sortable-silt) fraction tends to vary independently of sediment supply in current-sorted muds in the world's oceans, with coarser sediments representing relatively greater near-bottom flow speeds. Traditionally, the coarseness of this size fraction is described using an index called sortable-silt mean size ($\overline{SS}$), which is an arithmetic average calculated from the *differential volume* or *mass distribution* of grains within the 10–63 μm terrigenous silt fraction, where the relative weights of the individual size bins become increasingly disproportionate, with respect to the actual number of grains within those size bins, toward the coarse end of the size range. This not only increases the absolute value of the apparent "mean size" within the 10–63 μm terrigenous silt fraction, but it may also affect the apparent pattern of relative changes in the coarseness of the sortable-silt fraction along the core. In addition, it makes $\overline{SS}$ more prone to biases due to, for example, analytical errors. Here we present a detailed analysis of grain-size distributions over three selected Holocene time intervals from two complementary sediment cores (JM97-948/2A and MD95-2011), extracted from the center of a high-accumulation area along the flow path of the main branch of the Atlantic Inflow into the Nordic Seas and show that differential-number-based statistics, which likely better describes variations in the actual coarseness of the sortable-silt fraction, may provide a more robust alternative to $\overline{SS}$.

1. Introduction

Changes in the coarseness of the 10–63 μm terrigenous silt (i.e., sortable-silt) fraction of marine sediments, across successive layers of current-sorted deposits, are considered to be good indicators of past variations in the strength of the depositing current, with coarser sediments indicating intervals of relatively greater near-bottom flow speeds [*McCave and Hall*, 2006; *McCave et al.*, 1995]. The sortable-silt signal is thought to arise mainly from selective deposition as some grains (and aggregates) are trapped in the viscous sublayer of the turbulent boundary layer just above the seafloor, while others of smaller settling velocity are kept in turbulent suspension and transported further downcurrent [*McCave and Hall*, 2006; *McCave et al.*, 1995]. Ocean currents can rarely move terrigenous grains larger than 63 μm [*McCave and Hall*, 2006], which thus defines the upper limit of the size range that can provide information about the past strength of the flow. However, not all grains smaller than 63 μm are suitable for our purposes. In contrast to coarse silt (10 μm $< d <$ 63 μm), fine-silt and clay particles ($d <$ 10 μm) tend to behave cohesively, thus when the current is mobilizing, transporting, or depositing them it is acting on aggregates (i.e., groups of particles), rather than individual grains [*McCave and Hall*, 2006; *McCave et al.*, 1995]. Yet we can analyze sediments with scientific rigor only in their disaggregated state. Therefore, we truncate the grain-size distribution at 10 μm and exclude the fine-silt and clay component from the analysis.

The coarseness of the sortable-silt fraction is most often described using an index called "sortable-silt mean size ($\overline{SS}$)" [e.g., *Ellison et al.*, 2006; *Hoogakker et al.*, 2011; *McCave et al.*, 1995; *Praetorius et al.*, 2008; *Thornalley et al.*, 2013], which is an arithmetic average calculated from the *differential volume* or *mass (weight) distribution* of grains within the 10–63 μm terrigenous silt fraction. Even though $\overline{SS}$ does not reflect the characteristic physical size of the grains within the sortable-silt fraction, since it is not based on the number count of grains within the sample, in the literature the term "sortable-silt mean size" is often interchangeably used with "mean grain size," which is misleading.

While Coulter Counters have a long history in fine-grained current-sorted deep-sea sediment analysis [*Ledbetter and Johnson*, 1976], reliance on volume and mass (weight) distributions, as opposed to number-

frequency distributions, has remained the norm to date in this field. This approach likely has its roots in the past, since in the early days, using conventional approaches such as the Atterberg method and the pipette technique [*McCave and Syvitski*, 1991; *Stein*, 1985], it was simply not possible to count fine sediment grains. Furthermore, among modern instruments the SediGraph has been the preferred choice in the analysis of current-sorted sediments, in part because the corresponding measurement method rests on the settling velocity principle [*Coakley and Syvitski*, 1991]. Therefore, it is considered to yield a "dynamical" grain-size distribution closely related to transport and depositional processes [*McCave*, 2007; *McCave and Hall*, 2006]. However, the SediGraph cannot count grains either. While the Coulter Counter relies on the electrical sensing zone method, a fundamentally different measurement technique, *Bianchi et al*. [1999] showed that it provides equally precise and accurate determination of "mean size" based on the mass (weight) distribution of grains within the samples as the SediGraph, and even more precise and accurate results when the sortable-silt fraction is less than 5 wt % of the fine fraction of the sediment. Therefore, choosing the Coulter Counter over the SediGraph, in order to be able to use number-frequency distributions in the analysis of current-sorted deposits, does not compromise the quality of the data.

Over the past decades numerous studies have been devoted to understanding the physics controlling erosion, sediment transport, and deposition, including laboratory experiments, field observations, and theoretical treatment of the subject [e.g., *Dade et al*., 1992; *Fugate and Friedrichs*, 2003; *Gross and Williams*, 1991; *Hunt*, 1986; *McCave and Swift*, 1976; *Mehta and Lott*, 1987; *Self et al*., 1989], and identifying the instruments/methods best suited to fine-grained sediment analysis [e.g., *Bianchi et al*., 1999; *McCave et al*., 2006; *Singer et al*., 1988; *Stein*, 1985; *Syvitski et al*., 1991]. However, even though $\overline{SS}$ cannot directly (i.e., on a theoretical level) be linked to the physical processes described by *McCave et al*. [1995], *McCave and Hall* [2006], and others, to the best of our knowledge, the implications of the underlying volume or mass (weight)-based grain-size distributions for paleo-flow reconstructions have not yet been investigated.

Here we present a simple but detailed analysis of sortable-silt records from the eastern Nordic Seas to demonstrate how our choice of statistics can bear upon our conclusions regarding the past behavior of the depositing current. We based our calculations on measurements taken on two complementary sediment cores, IMAGES piston core MD95-2011 and box core JM97-948/2A (66°58.19′N, 07°38.36′E, water depth: 1048 m), which had been extracted from a Holocene high-accumulation area (HA) on the mid-Norwegian Margin along the flow path of the main branch of the Atlantic Inflow into the Nordic Seas, the Norwegian Atlantic Slope Current (NwASC, Figure 1a). We present two alternative time series based on exactly the same set of measurements for the interval between 9500 and 7500 years B.P. (early Holocene) and the past approximately 4150 years (late Holocene) (Figure 2). The two records are alternative representations of changes in the coarseness of the 10–63 μm terrigenous silt fraction of the sediments at our site through time.

The traditionally used sortable-silt mean size ($\overline{SS}$) is an arithmetic average computed from the *differential volume* distribution of grains within a sample:

$$\overline{SS} = \frac{1}{V}\sum_{i=1}^{256}(V_i \cdot d_i), \tag{1}$$

where

d_i is the midpoint value of the ith size bin ($i = 1, 2, 3, \ldots, 256$): 10 μm $< d_i <$ 63 μm;

V_i is the total volume of all the grains that fall into the ith size bin ($i = 1, 2, 3, \ldots, 256$);

V is the total volume of all (i.e., approximately 70,000) grains measured per sample:

$$V = \sum_{i=1}^{256} V_i. \tag{2}$$

Note that in equation (1), the weights $\left(\frac{V_i}{V}\right)$ of the individual size bins become increasingly disproportionate, with respect to the actual number of grains within those size bins, toward the coarse end of the grain-size distribution. When calculating an arithmetic mean from the *differential volume* distribution of grains within our sample a single 63 μm grain will have a 250 times larger weight in the average than a 10 μm grain based on their respective volumes $\left(V_{grain} = \frac{4}{3}\pi\left(\frac{d}{2}\right)^3\right)$ as opposed to computing a mean size from the *differential number* distribution of grains within the same sample, where each grain counts as one irrespective of its size.

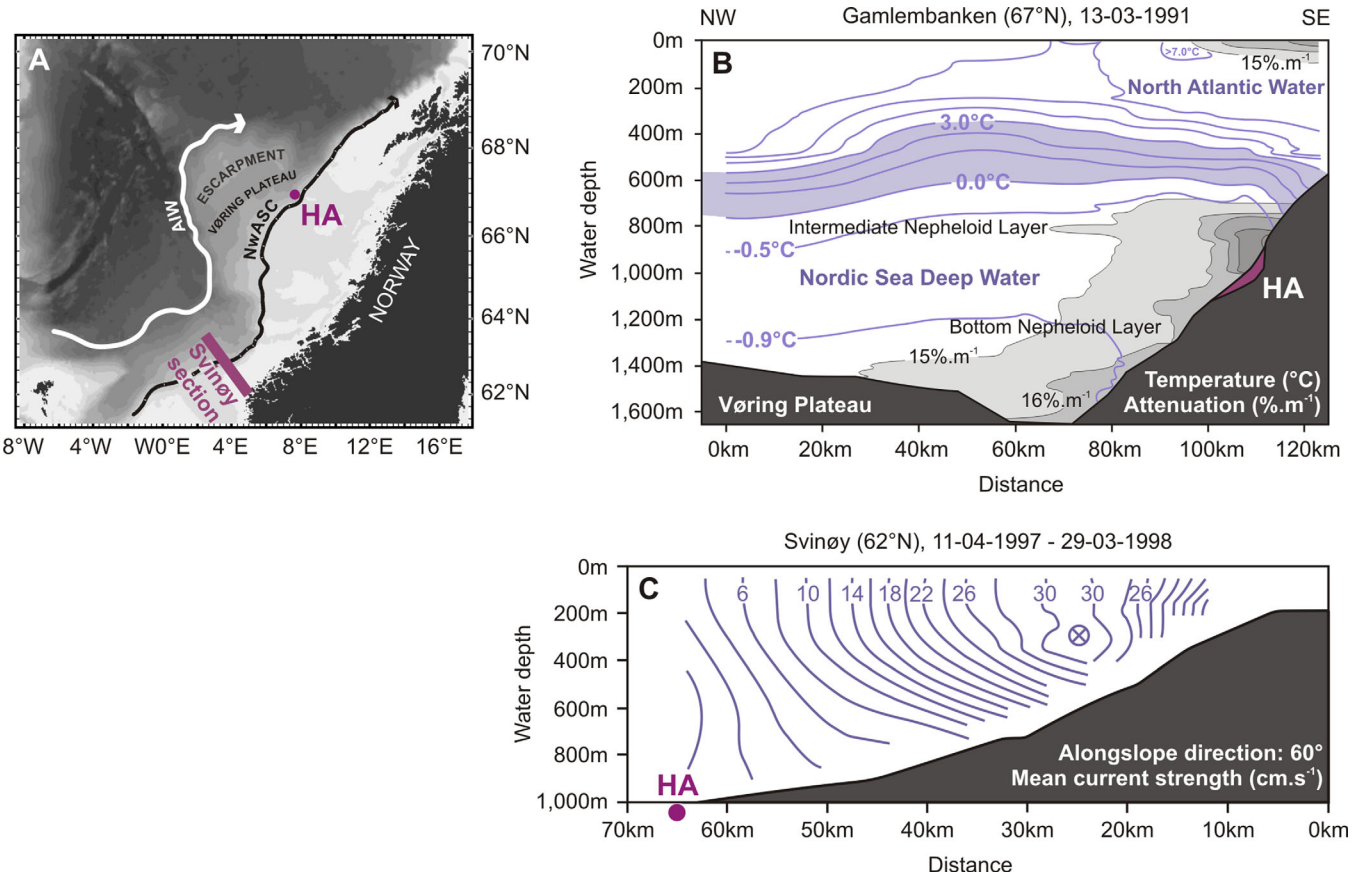

Figure 1. (a) Map of the wider study area. Our coring location ("HA") is marked by the purple dot. The segment of the Svinøy section corresponding to Figure 1c is also shown [*Mork and Skagseth*, 2010]. The flow path of the Norwegian Atlantic Slope Current (NwASC) is indicated by the black arrow [*Orvik and Niiler*, 2002]. This (sub)surface current is tracking the shelf break and has a flow depth of 600–800 m [*Hjøllo*, 1999; *Mauritzen*, 1996; *Mork and Skagseth*, 2010; *Rumohr et al.*, 2001]. The main geostrophic current in Arctic Intermediate Water (AIW) at approximately 1000 m water depth is marked by the white arrow. It is tracking the slope to the west of the Vøring Escarpment, not the continental slope to the east (i.e., below the main shelf break) [*Voet et al.*, 2010]. The basemap was generated by GeoMapApp© 3.3.0 [*Ryan et al.*, 2009]. (b) A nepheloid layer (in light to medium gray) in the downslope channel off Gamlembanken as observed on 13 March 1991 ("Poseidon" cruise 181). Note the densest part of the plume over the HA. The temperature profile of the water column is also shown. Most authors define the base of the NwASC as the 3°C isoline. The transition "zone" between Atlantic Waters and underlying deep waters are marked by the light-blue shading between the 3°C and 0°C isolines. Figure modified from *Rumohr et al.* [2001]. (c) The mean slope-parallel velocity field across the Svinøy section (62°N, for location see Figure 1a) between 11 April 1997 and 29 March 1998. The velocity profile at our site is likely very similar to that observed at the Svinøy section. Therefore, we indicated the relative depth of our site (purple circle) with respect to the (sub)surface flow (for the actual location of our site relative to the Svinøy section see Figure 1a). Modified from *Hjøllo* [1999] with kind permission from *Solfrid Sætre Hjøllo* and *Øystein Skagseth*.

In order to avoid misleading or confusing terminology and to emphasize that $\overline{SS}$ does not reflect the actual physical size of the average grain within the 10–63 μm terrigenous silt fraction, we will refer to this number as the sortable-silt index throughout the paper.

We also calculated "sortable-silt mean grain diameter ($\bar{d}_{SS}$)" for every sample, using exactly the same raw Coulter Counter output as for computing the sortable-silt index (Figure 2). This is also an arithmetic average, but it is based on the *differential number* distribution of grains within the sample:

$$\bar{d}_{SS} = \frac{1}{N}\sum_{i=1}^{256}(N_i \cdot d_i), \tag{3}$$

where

d_i is the midpoint value of the ith size bin ($i = 1, 2, 3, \ldots, 256$): 10 μm $< d_i <$ 63 μm;

N_i is the number of grains that fall into the ith size bin ($i = 1, 2, 3, \ldots, 256$);

N is the total number of grains measured per sample (i.e., approximately 70,000):

$$N = \sum_{i=1}^{256} N_i. \tag{4}$$

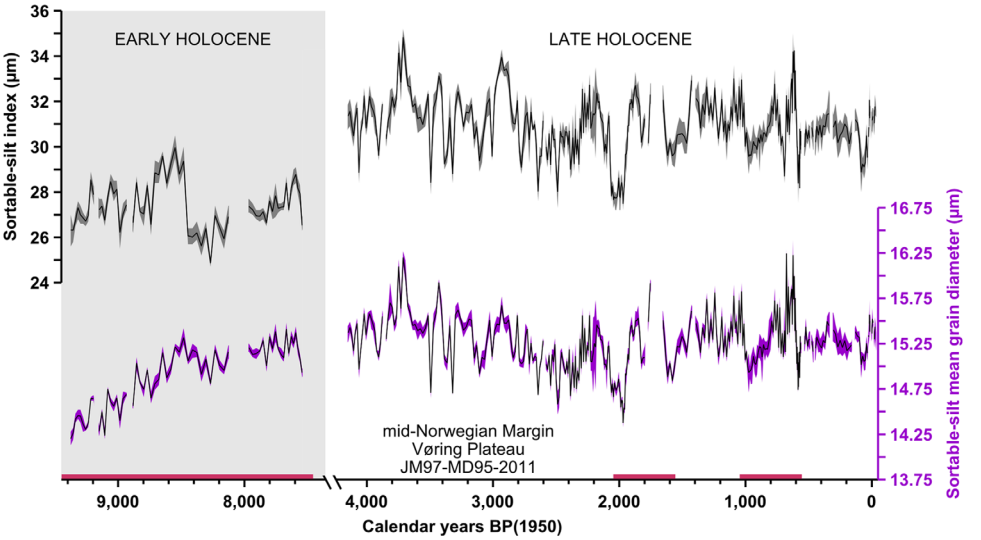

Figure 2. The two alternative sortable-silt time series from sediment cores JM97-948/2A and MD95-2011. Note the fourfold difference in scale between the records. The shaded envelopes indicate the spread of values resulting from repeated measurements. The mean $\pm 1\sigma$ error in the age model is $\pm$128 years over the late Holocene and $\pm$201 years over the early Holocene. The present study focuses on the three intervals highlighted in purple along the time axis (9500–7500, 2050–1550, and 1050–550 years B.P.).

Sortable-silt mean grain diameter better approximates the actual physical size of the average grain in the 10–63 μm terrigenous silt fraction than the sortable-silt index. Hence, $\bar{d}_{SS}$ may be more closely related to the physical processes that produced the grain-size distribution of the sampled sediment horizon than $\overline{SS}$.

Figure 3 illustrates the differences between the two statistical approaches. The differential number distribution is logarithmic and tails off very rapidly. Thus, $\bar{d}_{SS}$ falls close to the lower limit of the 10–63 μm size range. Weighing the size bins with differential volume flattens the distribution and shifts the mean ($\overline{SS}$) toward significantly higher values, which thus suggests a much stronger flow. When comparing $\overline{SS}$ to the differential number distribution, it is easy to see that most grains in the sample are much smaller in diameter than that suggested by the sortable-silt index.

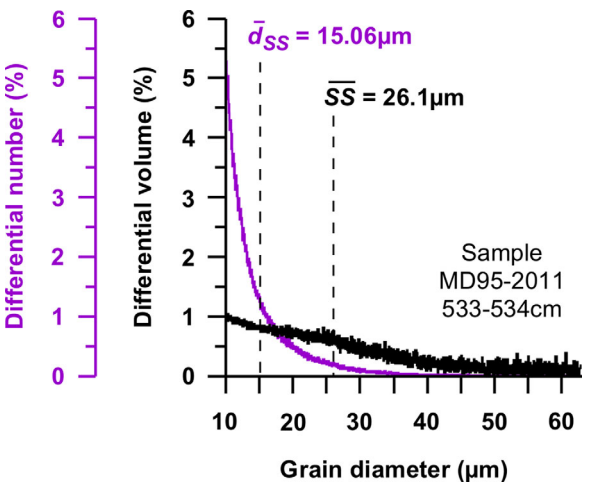

Figure 3. A comparison of the differential number and differential volume distribution of grains within the same early Holocene sample and the respective arithmetic averages, namely mean grain diameter ($\bar{d}_{SS}$) and the sortable-silt index ($\overline{SS}$).

2. Oceanographic Setting and Sedimentary Processes

The NwASC is a strong, topographically trapped shelf-edge current [*Mork and Skagseth*, 2010; *Orvik and Niiler*, 2002], which is winnowing the shelf and upper continental slope along the Norwegian Margin (Figure 1a) [*Dahlgren and Vorren*, 2003; *Holtedahl*, 1981; *Laberg et al.*, 2005]. Hydrographic sections (Figure 1b) [*Rumohr et al.*, 2001] and velocity profiles (Figure 1c) [*Hjøllo*, 1999] indicate that in the modern ocean it reaches down to about 600–800 m water depth. In contrast, our site is located at a water depth of 1048 m (Figure 1b) [*Rumohr et al.*, 2001]. At this depth, the main geostrophic flow from the Norwegian Basin into the Lofoten Basin tracks the 2000 m bathymetric contour and is guided along the western slope of the

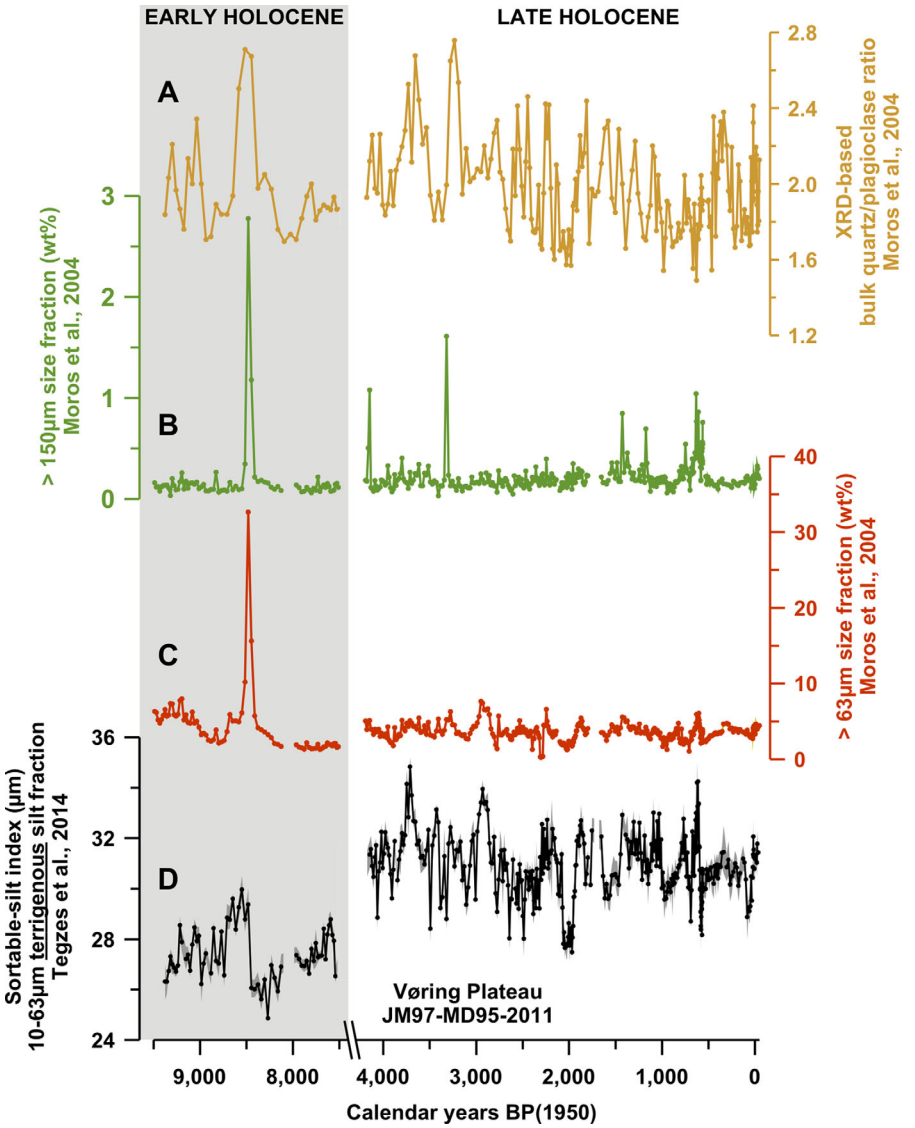

Figure 4. Sortable silt and IRD input. All records are from our site (box core JM97-948/2A and piston core MD95-2011). Two time intervals are shown: 9500–7500 years B.P. (early Holocene) and 4200 years B.P. to present (late Holocene). (a) XRD-based bulk quartz/plagioclase ratios, suggested as a complementary approach to mechanical separation and manual counting of terrigenous grains >150 μm in identifying IRD events by *Moros et al.* [2004b]. Note that this record has lower resolution (measurements were taken only on every other sample) than the others [*Moros et al.*, 2004a; M. Moros, personal communication, 2012]. (b) Changes in the weight percent of the >150 μm size fraction in bulk sediments along the two cores [*Moros et al.*, 2004a; Moros, personal communication, 2012; B. Risebrobakken, personal communication, 2012; C. Andersson, personal communication, 2014]. (c) Changes in the weight percent of the >63 μm size fraction in bulk sediments along the two cores [*Moros et al.*, 2004a; Moros, personal communication, 2012; Risebrobakken, personal communication, 2012; Andersson, personal communication, 2014]. (d) Changes in the coarseness of the 10–63 μm terrigenous silt fraction as reflected by the differential-volume-distribution-based sortable-silt index ($\overline{SS}$). We chose $\overline{SS}$ of the two sortable-silt proxies for consistency with graphs b and c.

Vøring Margin (Figure 1a) [*Voet et al.*, 2010], that is, at intermediate depth, there are no currents that could rework the sediments deposited at the HA. We hypothesize that the primary, NwASC-sorted deposits form in the upper segment of the cross-slope channel that runs downslope from Gamlembanken, over which the flow seems to slow down [*Rumohr et al.*, 2001; *Søiland et al.*, 2008]. The NwASC is in direct contact with the bed here (Figure 1b). These primary deposits are continuously being delivered down to the HA, which can be found in the lower segment of the same gully. Thus, according to our theory, the sediments at the HA represent secondary deposits. Low-density, hence low-energy turbidity plumes (not to be confused with turbidity currents) provide the necessary delivery mechanism from the upper slope down to our coring site, where they are likely brought to an abrupt halt. The triggering mechanisms and properties of these

turbidity plumes, described in detail by *Fohrmann et al*. [1998, 2001], make us hypothesize that these do not add another systematic multidecadal to multicentennial signal, in addition to the NwASC-strength signal, to the deposits at the HA.

While our site has been affected by ice-rafting events in the past [*Moros et al*., 2004a; Risebrobakken, personal communication, 2012], a comparison of our sortable-silt data with other proxy records from the same cores suggests that these have not corrupted the current-strength signal (Figure 4). The NwASC was probably weaker during the early Holocene than the late Holocene (Figure 4d). Therefore, its capacity to rework large amounts of sediments dumped onto the upper continental slope or to hinder the settling of particles in the upper water column over our site was likely smaller in the early Holocene (Figure 1b). Thus, the probability that a major ice-rafting event could overprint the current-strength signal at our coring location must have been larger between 9500 and 7500 years B.P. than over the past 4200 years. By far, the largest (verified) IRD event recorded in our cores over the intervals of interest occurred at around 8441 $\pm$ 201 years B.P. (Figures 4a–4c) [*Moros et al*., 2004a; Moros, personal communication, 2012; Risebrobakken, personal communication, 2012]. Yet there is no evidence that this affected the coarseness of the sortable-silt fraction (Figure 4d) [*Tegzes et al*., 2014].

In contrast to the early Holocene, the weight percent of the >63 μm size fraction exhibits some apparent similarities to the sortable-silt-index time series over the past 4200 years (Figures 4c and 4d). The fact that over the late Holocene there is weak or no correlation between the weight percent of the coarse fraction and bulk quartz/plagioclase ratios could potentially indicate that a significant part of the variability in the weight percent of the >63 μm size fraction may be due to changes in the biogenic component of the sediment (Figures 4a and 4c). This may either reflect past fluctuations in local productivity (i.e., past variations in the number of dead organisms settling out of the water column above our site), or changes in sediment-transport mechanisms with the capacity to deliver foraminiferal sand to our coring location. The NwASC plays a key role in both the climate and ecology of the region. Variations in its properties may significantly influence local productivity. Furthermore, considering that the NwASC is a highly competent current, it may have at times been strong enough over the late Holocene to mobilize foraminiferan tests along with coarse terrigenous silt grains [*McCave*, 2007; *Miller and Komar*, 1977; *Oehmig*, 1993]. While the second phase of sediment delivery to our site may complicate the picture, if foraminiferan sand and coarse terrigenous silt are truly transport-equivalent [*Oehmig*, 1993], then turbidity plumes should be able to mobilize these deposits too.

3. Methods

The split cores were sampled at 1 cm intervals. Bulk samples were wet sieved to separate the fine ($d < 63$ μm) from the coarse fraction ($d > 63$ μm). The dried and disaggregated fine fractions were subsampled and, in order to remove the biogenic component [*McCave and Hall*, 2006], were decarbonated and desilicated, using 1 *M* acetic acid and 2 *M* sodium carbonate solution, respectively. The decarbonated and desilicated fine fractions were stored in 0.02 *M* sodium polyphosphate solution in a cold room until measurement. They were then disaggregated, further subsampled and run on a Beckman Coulter® Multisizer™ 3, fitted with a 140 μm aperture tube, using Beckman Coulter ISOTON® II diluent. They were measured several times, each time in a different random order, at a concentration of 5–10% and a stirrer speed of 40 (before deciding on these settings we tested both the effect of sample concentration and stirrer speed on our results). The target size range was set to 10–63 μm, excluding the fine-silt and clay component [*McCave and Hall*, 2006; *McCave et al*., 1995].

The pulse data (i.e., the raw Coulter Counter output) were saved following each run, and were later converted into a *differential volume* and a *differential number* distribution, using 256 equal size bins. The size bins were defined in grain diameters (d) in micrometers. These distributions served as a basis for calculating $\overline{SS}$ and $\bar{d}_{SS}$, respectively.

4. Results

4.1. Relative Changes in the Coarseness of the Sediment

While in general, the two sortable-silt records are in good agreement as far as relative changes are concerned, there are some major differences between the two time series, most strikingly the relative

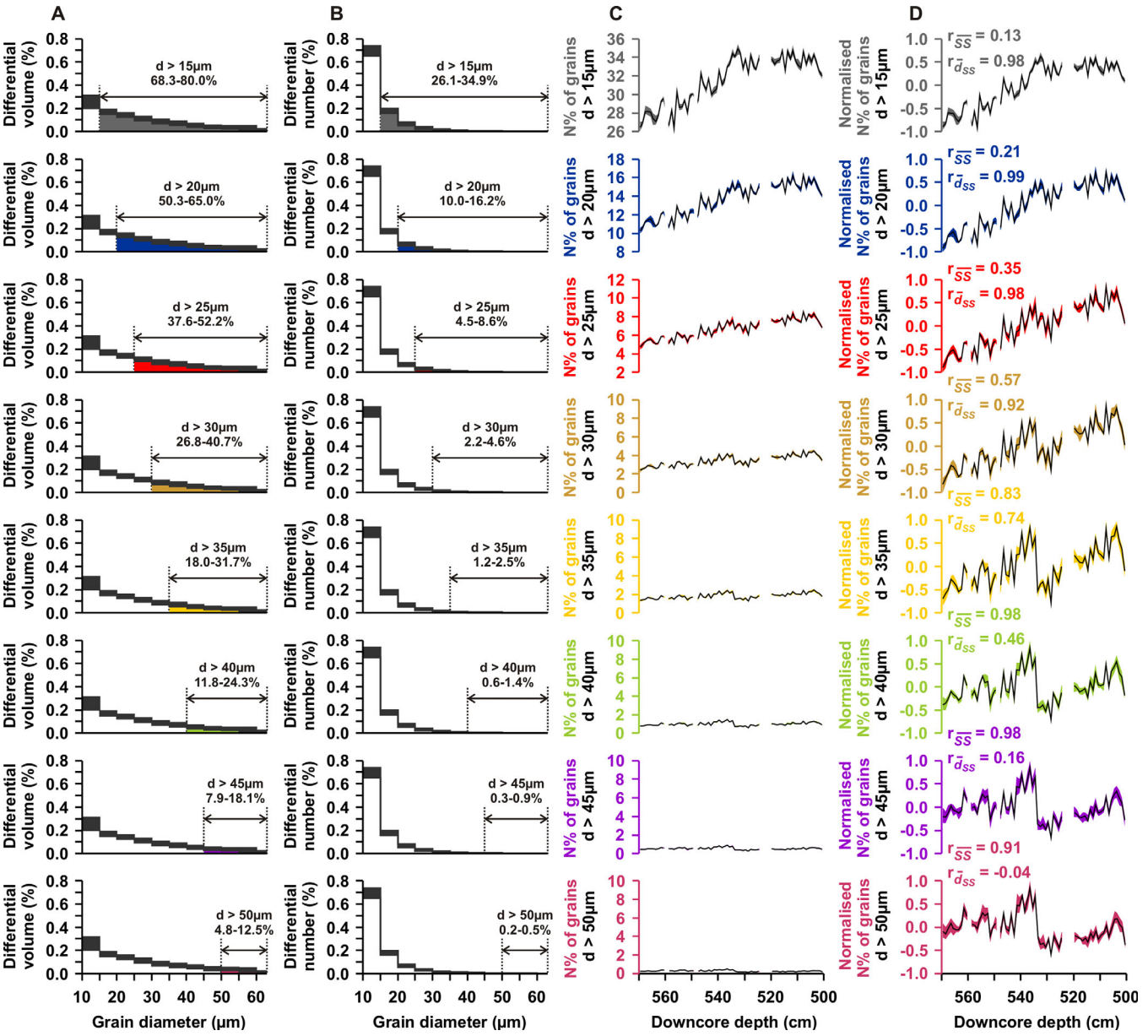

Figure 5. Interval: 9500–7500 years B.P. (column a) The characteristic differential volume distribution of grains over the interval and the volume percent of grains that make up the progressively coarser tail (>15, >20, >25, . . . , >50 μm) of the distribution. (column b) The characteristic differential number distribution of grains over the interval and the number percent of grains that make up the progressively coarser tail (>15, >20, >25, . . . , >50 μm) of the distribution. The dark gray "caps" on top of the bars in the step plots in columns a and b indicate the range of values for each size bin over the interval. (column c) Records of the percentage-based enrichment of grains with d >15 μm, >20 μm, etc., to total sortable-silt (10–63 μm) fraction from the original 256-size-bin Coulter Counter output. All graphs are to scale. (column d) Normalized records of the percentage-based enrichment of grains with d > 15 μm, >20 μm, etc., to total sortable-silt (10–63 μm) fraction from the original 256-size-bin Coulter Counter output. The correlation coefficients quantify the similarity of trends in the percentage-based enrichment of respective coarse grains and sortable-silt index values ($r_{\overline{SS}}$), and between the percentage-based enrichment of respective coarse grains and sortable-silt mean grain diameters ($r_{\bar{d}_{ss}}$). In each record in columns c and d, the shaded envelope indicates the spread of values resulting from repeated measurements.

magnitude and temporal evolution of the event at approximately 8500 ± 201 years B.P. (Figure 2). The present study focuses on the three intervals, highlighted along the time axis in Figure 2 (9500–7500, 2050–1550, and 1050–550 years B.P.).

For the purposes of this analysis, we divided the 10–63 μm size range into 11 size bins (10–15, 15–20, 20–25, . . . , 60–63 μm). For each time slice (9500–7500, 2050–1550, and 1050–550 years B.P.), we calculated a characteristic differential number distribution using the samples that gave the respective minima and maxima within those intervals (column b in Figures 5–7). We then calculated the number percent of grains that made up the progressively coarser tail (>15, >20, >25, . . . , >50 μm) of those distributions (column b in

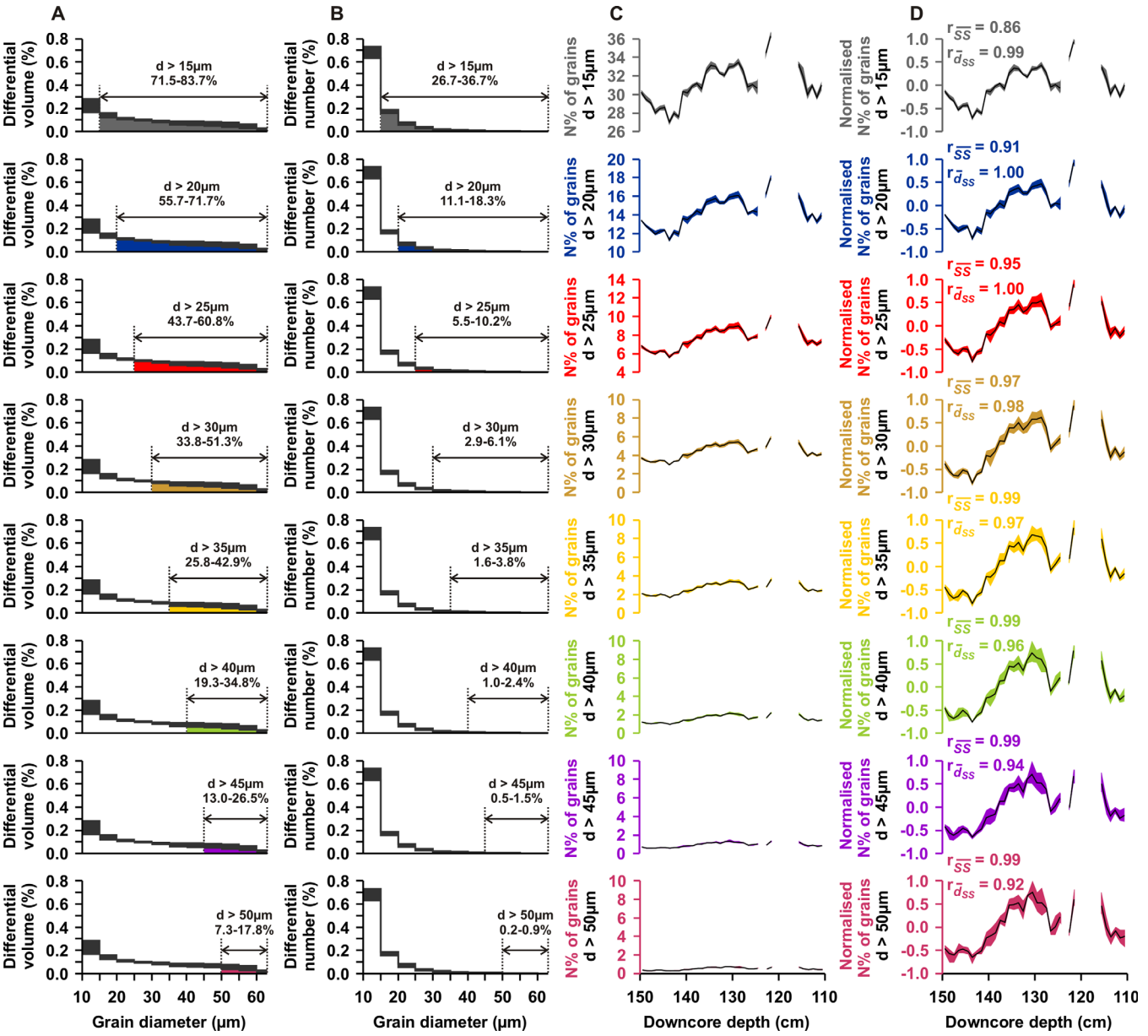

Figure 6. Interval: 2050–1550 years B.P. (column a) The characteristic differential volume distribution of grains over the interval and the volume percent of grains that make up the progressively coarser tail (>15, >20, >25, . . . , >50 μm) of the distribution. (column b) The characteristic differential number distribution of grains over the interval and the number percent of grains that make up the progressively coarser tail (>15, >20, >25, . . . , >50 μm) of the distribution. The dark gray "caps" on top of the bars in the step plots in columns a and b indicate the range of values for each size bin over the interval. (column c) Records of the percentage-based enrichment of grains with d >15 μm, >20 μm, etc., to total sortable-silt (10–63 μm) fraction from the original 256-size-bin Coulter Counter output. All graphs are to scale. (column d) Normalized records of the percentage-based enrichment of grains with d > 15 μm, >20 μm, etc., to total sortable-silt (10–63 μm) fraction from the original 256-size-bin Coulter Counter output. The correlation coefficients quantify the similarity of trends in the percentage-based enrichment of respective coarse grains and sortable-silt index values ($r_{\overline{ss}}$), and between the percentage-based enrichment of respective coarse grains and sortable-silt mean grain diameters ($r_{\bar{d}_{ss}}$). In each record in columns c and d, the shaded envelope indicates the spread of values resulting from repeated measurements.

Figures 5–7). We found that in general 65–75% of the grains were smaller than 15 μm in diameter and only less than 1% were larger than 50 μm.

For each coarse tail (>15, >20, >25, . . . , >50 μm), we then extracted the percentage of respective grains (i.e., those with d > 15 μm, >20 μm, etc.) within the total sortable-silt fraction (10–63 μm) from the original 256-size-bin Coulter Counter output for all samples within the selected time intervals. We analyzed both the absolute percentage-point changes (column c in Figures 5–7), and also the normalized records (column d in Figures 5–7): the former to investigate how a progressively coarser tail affected the amplitude of variability, the latter to compare the pattern of change along the core between the different coarse tails.

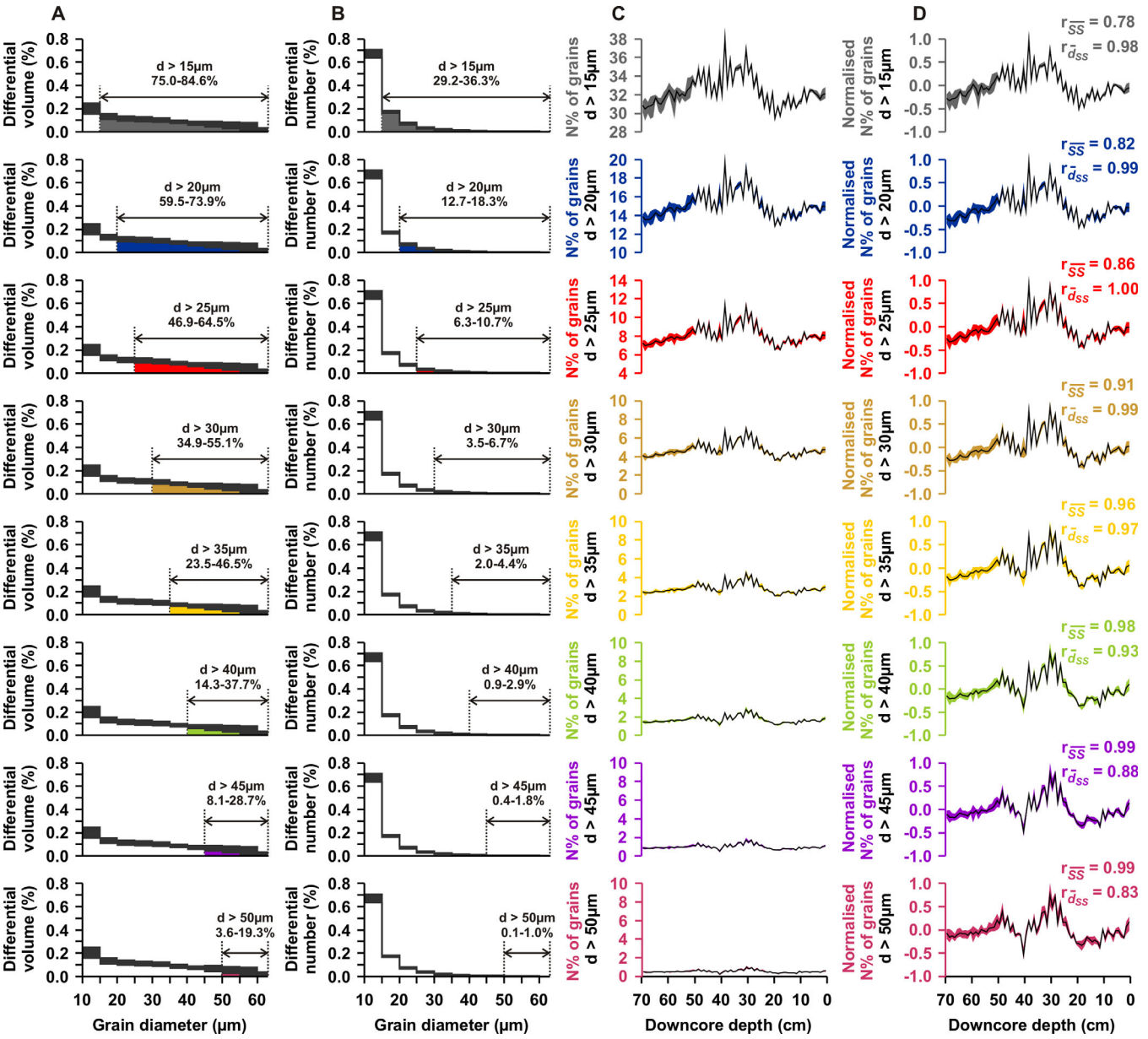

Figure 7. Interval: 1050–550 years B.P. (column a) The characteristic differential volume distribution of grains over the interval and the volume percent of grains that make up the progressively coarser tail (>15, >20, >25, . . . , >50 μm) of the distribution. (column b) The characteristic differential number distribution of grains over the interval and the number percent of grains that make up the progressively coarser tail (>15, >20, >25, . . . , >50 μm) of the distribution. The dark gray "caps" on top of the bars in the step plots in columns a and b indicate the range of values for each size bin over the interval. (column c) Records of the percentage-based enrichment of grains with $d > 15$ μm, >20 μm, etc., to total sortable-silt (10–63 μm) fraction from the original 256-size-bin Coulter Counter output. All graphs are to scale. (column d) Normalized records of the percentage-based enrichment of grains with $d > 15$ μm, >20 μm, etc., to total sortable-silt (10–63 μm) fraction from the original 256-size-bin Coulter Counter output. The correlation coefficients quantify the similarity of trends in the percentage-based enrichment of respective coarse grains and sortable-silt index values ($r_{\overline{SS}}$), and between the percentage-based enrichment of respective coarse grains and sortable-silt mean grain diameters ($r_{\bar{d}_{SS}}$). In each record in columns c and d, the shaded envelope indicates the spread of values resulting from repeated measurements.

Using *normalized mean values*, we calculated correlation coefficients between the percentage of coarse grains and $\overline{SS}$ ($r_{\overline{SS}}$), and between the percentage of coarse grains and $\bar{d}_{SS}$ ($r_{\bar{d}_{SS}}$) for each coarse tail (column d in Figures 5–7; summarized in Tables (1–3)). We found that while $\bar{d}_{SS}$ most strongly correlated with the percentage of grains >20–25 μm (representing 6–18% of the sortable-silt fraction; columns b and d in Figures 5–7), $\overline{SS}$ most strongly correlated with the percentage of grains >45 μm (representing <2% of the sortable-silt fraction, i.e., a couple of hundred grains out of the 69,000–75,000 measured per sample; columns b and d in Figures 5–7). Whereas variations in the correlation coefficients were relatively subtle with overall coarser sediments representing the late Holocene (2050–1550 and 1050–550 years B.P.), the

Table 1. Tabulated Correlation Coefficients for the Interval 9500–7500 Years B.P.[a]

	N% of Grains Within the Sortable-Silt Fraction							
	$d > 50$ μm	$d > 45$ μm	$d > 40$ μm	$d > 35$ μm	$d > 30$ μm	$d > 25$ μm	$d > 20$ μm	$d > 15$ μm
$\overline{SS}$	0.9063	**0.9782**	**0.9782**	0.8260	0.5715	0.3546	0.2129	0.1257
$\bar{d}_{SS}$	−0.0397	0.1574	0.4558	0.7436	0.9209	0.9840	**0.9936**	0.9784

[a]The highest correlation coefficients are highlighted in bold font.

Table 2. Tabulated Correlation Coefficients for the Interval 2050–1550 Years B.P.[a]

	N% of Grains Within the Sortable-Silt Fraction							
	$d > 50$ μm	$d > 45$ μm	$d > 40$ μm	$d > 35$ μm	$d > 30$ μm	$d > 25$ μm	$d > 20$ μm	$d > 15$ μm
$\overline{SS}$	0.9918	**0.9929**	0.9908	0.9866	0.9734	0.9487	0.9122	0.8606
$\bar{d}_{SS}$	0.9182	0.9403	0.9565	0.9684	0.9838	0.9953	**0.9978**	0.9875

[a]The highest correlation coefficients are highlighted in bold font.

Table 3. Tabulated Correlation Coefficients for the Interval 1050–550 Years B.P.[a]

	N% of Grains Within the Sortable-Silt Fraction							
	$d > 50$ μm	$d > 45$ μm	$d > 40$ μm	$d > 35$ μm	$d > 30$ μm	$d > 25$ μm	$d > 20$ μm	$d > 15$ μm
$\overline{SS}$	0.9852	**0.9909**	0.9826	0.9559	0.9140	0.8623	0.8183	0.7802
$\bar{d}_{SS}$	0.8271	0.8787	0.9293	0.9697	0.9919	**0.9969**	0.9924	0.9806

[a]The highest correlation coefficients are highlighted in bold font.

differences were quite significant in the case of overall finer samples of early Holocene age (9500–7500 years B.P.) (Tables 1–3).

In order to further investigate the nature of $\overline{SS}$, similarly to the differential number distributions and using exactly the same samples, we also calculated typical differential volume distributions (column a in Figures 5–7) for the three time intervals discussed above (9500–7500, 2050–1550, and 1050–550 years B.P.). We then compared the two types of distributions (differential volume (column a in Figures 5–7) versus differential number (column b in Figures 5–7)) and found that the bias in the weight of the coarse tail of the distribution increased from (2.2–2.7)-fold in the case of grains with $d > 15$ μm to (19.0–34.7)-fold in the case of grains with $d > 50$ μm when using differential volume instead of differential number (Table 4). This can explain how the $\overline{SS}$ time series can be determined by variations in just a small fraction of the grains, i.e., those with $d > 45$ μm.

4.2. Sedimentation During Measurement

There is almost always some degree of sedimentation during measurement, even if it is not strikingly obvious to the naked eye. Therefore, as indicated before, we carried out a "speed test" using the samples covering the 2050–1550 years B.P. interval when setting up the Coulter Counter (Figure 8). We increased the stirrer (Figure 9) speed from an initial value of 20 up to 40. Beyond that the stirrer started generating a

Table 4. The Relative Weight of the Coarse Tail of the Grain-Size Distribution[a]

	Coarse Tail: Grains With $d > 15$ μm			Coarse Tail: Grains With $d > 50$ μm		
	The Relative Weight of the Coarse Tail			The Relative Weight of the Coarse Tail		
Interval	Based on Differential Number Distributions	Based on Differential Volume Distributions	The Increase in the Relative Weight of the Coarse Tail When Switching to Differential-Volume-Based Statistics	Based on Differential Number Distributions	Based on Differential Volume Distributions	The Increase in the Relative Weight of the Coarse Tail When Switching to Differential-Volume-Based Statistics
9500–7500 years B.P.	26.1–34.9%	68.3–80.0%	2.2-fold to 2.7-fold	0.2–0.5%	4.8–12.5%	24.1-fold to 34.5-fold
2050–1550 years B.P.	26.7–36.7%	71.5–83.7%	2.3-fold to 2.7-fold	0.2–09%	7.3–17.8%	20.1-fold to 30.7-fold
1050–550 years B.P.	29.2–36.3%	75.0–84.6%	2.3-fold to 2.6-fold	0.1–1.0%	3.6–19.3%	19.0-fold to 27.8-fold

[a]Similarly to the characteristic differential volume and differential number distributions in columns a and b in Figures 5–7, the values in the table above were also calculated based on the samples that gave the respective minima and maxima within each selected time interval in the $\overline{SS}$ and $\bar{d}_{SS}$ records (Figure 2).

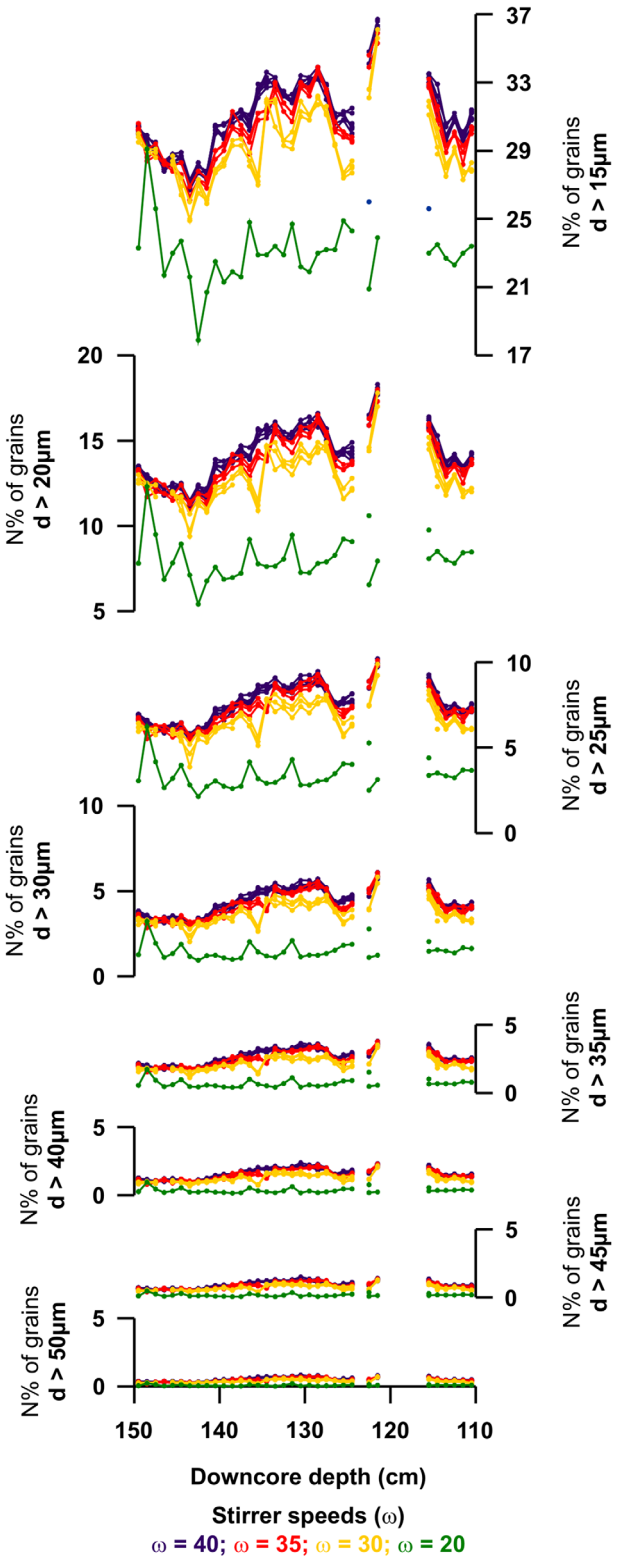

Figure 8. The impact of increasing the stirrer speed from 20 to 40 on the absolute percentage-point values and the pattern of change along the core (corresponding to the 2050–1550 years B.P. interval) in the weight of the progressively coarser tail of the differential number distribution of grains. All graphs are drawn to scale.

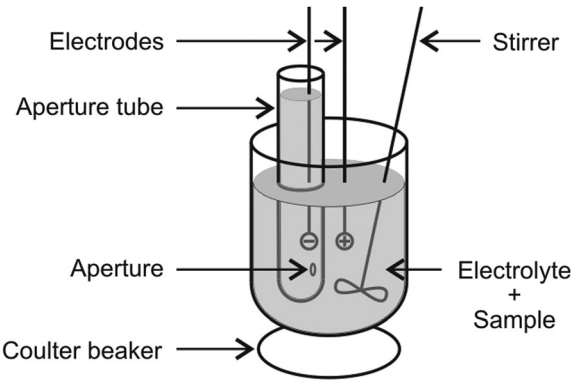

Figure 9. Cartoon of the basic setup inside the Coulter® Multisizer™ 3.

vortex and small bubbles, which occasionally corrupted the data. In addition, when increasing the stirrer speed from 35 to 40 results showed relatively little change (Figure 8).

It is interesting to see how sensitive even the relatively finer grains are to our stirrer settings. Due to the logarithmic shape of the differential number distribution, the number percent of the coarse tail with grains down to 15 μm in diameter shows the largest increase with increasing stirrer speed.

Evidently, the heaviest grains are the most difficult to keep in suspension throughout the duration of the entire measurement. In addition, their concentration is the lowest within the sample. Therefore, they are the most difficult to count accurately. This has particular significance in light of our result that changes in $\overline{SS}$ show the strongest correlation with variations in the percentage of grains $>$45 μm, while changes in $\bar{d}_{SS}$ show the strongest correlation with variations in the percentage of grains $>$20–25 μm, which makes the latter less susceptible to inaccuracies in the measurement of a small percentage of all the grains within the sortable-silt fraction.

5. Discussion

Most of the physics that serves as a basis for current-strength reconstructions is related to the parameters of individual grains, most notably their size. The actual coarseness of current-sorted deposits is represented by the (differential) number distribution of grains within the 10–63 μm terrigenous silt fraction. As we have shown earlier, there are many different ways in which to describe such a distribution with a single number. However, $\bar{d}_{SS}$ gives us the mean physical size of these grains, assuming they are approximately spherical in shape. In contrast, $\overline{SS}$ is greatly biased toward the largest grains within the distribution (Figure 3). While there seem to be issues with the use of (differential) volume or mass-based statistics even in the case of relative flow-strength reconstructions, it may prove to be particularly problematic for calibration studies, which aim to put an absolute scale on sortable-silt index ($\overline{SS}$) time series [*Thornalley et al.*, 2013].

For example, according to the typical differential number distribution of grains within the early Holocene part of our record, 91–95% of grains fall into the 10–25 μm size range (column b in Figure 5). Mean grain diameters vary between 15.02 and 15.42 μm, while the sortable-silt index fluctuates between 25.7 and 30.0 μm over the same period. Similarly, within the 1050–550 years B.P. interval typically 89–94% of grains have diameters between 10 and 25 μm. Mean grain diameters vary between 14.82 and 16.03 μm, while the sortable-silt index fluctuates between 27.8 and 34.5 μm over the same five centuries (column b in Figure 7). That is, $\overline{SS}$ implies a much stronger flow, since it suggests that the average grain deposited by the current is approximately two times larger than it actually is.

As far as time series are concerned, the differential-volume-weighted sortable-silt index does not simply amplify changes. The bias it introduces is not systematic and that affects the relative magnitude of variability through time in our current-strength proxy records (compare, e.g., the 9500–7500 years B.P. interval in plots 1a-1c in Figure 10, with the 1050–550 years B.P. interval in plots 2a-2c in Figure 10), which can thus reflect an altogether different physics. For example, looking at the event between 535 and 525 cm (~8500

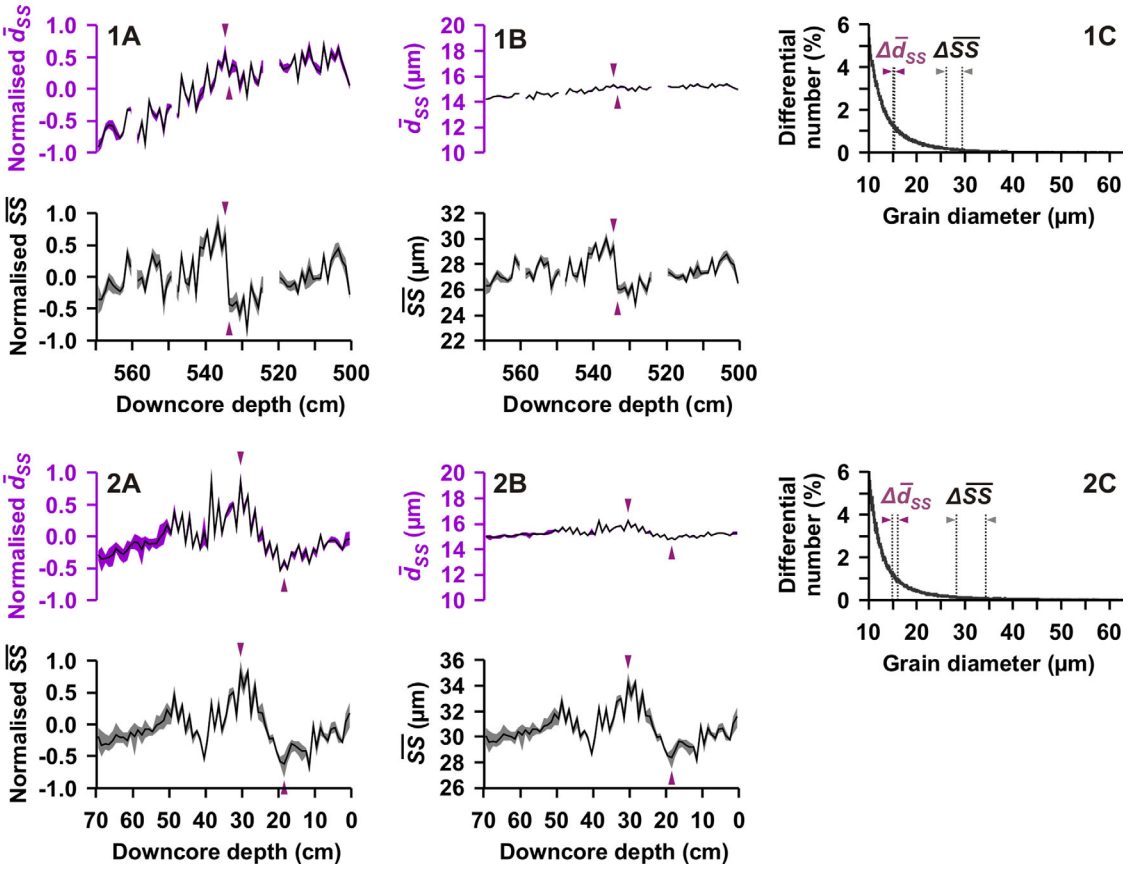

Figure 10. The bias introduced by using a differential-volume-weighted arithmetic average of grain sizes. Plots 1a–1c are based on data from the early Holocene (9500–7500 years B.P.), while Plots 2a–2c on samples of late Holocene age (1050–550 years B.P.). (column a) Normalized records of mean grain diameters ($\bar{d}_{SS}$) and sortable-silt index values ($\overline{SS}$) over the interval. (column b) Absolute changes in mean grain diameters and the sortable-silt index over the interval. Graphs are drawn to scale. (column c) Superimposed 256-size-bin differential number distributions based on samples that give the respective minimum and maximum, highlighted on the graphs in column b. Note the relative magnitude of the differential-number-weighted $\bar{d}_{SS}$ and the differential-volume-weighted $\overline{SS}$ values for both the maxima and the minima and the relative magnitude of the change from peak to trough in mean grain diameters ($\Delta\bar{d}_{SS}$) and in the sortable-silt index ($\Delta\overline{SS}$).

years B.P.) in our records (plot 1a in Figure 10), did the NwASC abruptly slow down as indicated by $\overline{SS}$ or was there only a smaller and more gradual decrease in current strength as suggested by $\bar{d}_{SS}$? Does the index or mean grain diameters reflect what actually happened? How easy it is to disrupt ocean circulation [*Tegzes et al.*, 2014]?

Although much depends on the actual shape of the grain-size distribution, in general, the finer the silt, the larger the relative weight of a few big grains in the differential-volume-weighted arithmetic average. Thus, relatively minor changes in their number can potentially result in misleadingly large fluctuations in the sortable-silt index. The smaller the number of grains that ultimately determine these changes, the less representative variations in $\overline{SS}$ are of changes in the overall coarseness of the entire current-sorted deposit (i.e., the 10–63 μm terrigenous size fraction) that the flow accumulated at a given location over a certain time interval, and the more prone this index is to "random effects."

5.1. Sedimentation Under the Influence of Ocean Currents

The strength of the flow, especially locally, may vary greatly on different time scales from hours to millennia [e.g., *Gross and Williams*, 1991]. Ideally, the current-strength proxy should be such that it reflects the typical behavior of the flow during the time period over which it is calculated. If (negligibly) brief infrequent instances of exceptionally strong flow with "extreme" sediment-transport capacity are able to "overprint" that signal then we will get a false impression of the past strength of the current and more importantly of its overall volume transport, which is probably better mirrored by the mean current than occasional peak flow, in particular on multidecadal or multicentennial time scales. Therefore, we need a measure that is less prone

to biases due to "freak events." In this respect, $\bar{d}_{SS}$ could be a more robust measure of current strength than $\overline{SS}$.

The downcurrent fining of deposits, as a consequence of limitations in sediment supply, may further complicate the use of $\overline{SS}$. This phenomenon is known to affect sands. However, there exists the possibility that it may also truncate the coarse end of the sortable-silt fraction [*McCave and Hall*, 2006]. If under such circumstances we rely on differential volume or mass-based statistics, this may both amplify apparent spatial differences in the coarseness of bottom sediments along the flow path of the current and increase random errors in $\overline{SS}$ where deposits are finer. Limited downcurrent fining would less affect $\bar{d}_{SS}$ thus it would likely yield more consistent results between sites.

In any case, however, where supply limitation is suspected, additional locations have to be sampled both upstream and downcurrent of the site in question. If $\bar{d}_{SS}$ values vary greatly under the same "uniform" flow, the site is not suitable for calibration studies, and may only be used in current-strength reconstructions in the context of parallel investigations at neighboring locations. If a common temporal pattern in $\bar{d}_{SS}$ emerges from these sites, we can at least qualitatively evaluate variations in the past strength of the flow. In such cases, calculating temporal variations in the number percent of the progressively coarser tail of the differential number distribution of grains within the sortable-silt fraction (as presented earlier, Figures 5–7) at each location and comparing the respective time series between sites may give an even more reliable picture than $\bar{d}_{SS}$ alone.

5.2. Sample Preparation and the Coulter Method

Some of the factors that may corrupt the $\overline{SS}$ signal relate to laboratory work. First, sediment samples intended for current-strength reconstructions are normally not processed in a clean laboratory and there is always a chance for contamination. With the sortable-silt index being so sensitive to the presence of a few large grains within the sample, this can easily corrupt the $\overline{SS}$ signal.

Second, there is almost always some degree of sedimentation when running samples on the Coulter Counter. Trivially, the largest and heaviest grains in the sample are the most difficult to keep in suspension throughout the entire duration of the measurement. In addition, their concentration is the lowest within the sample. Therefore, they are the most difficult to count accurately. Consequently, $\overline{SS}$ is likely more susceptible to measurement error than $\bar{d}_{SS}$.

Third, there is a "built-in" error in the Coulter method itself. Inside the instrument a tube with a tiny (in our case 140 μm diameter) aperture in its wall is immersed into a beaker filled with a mixture of electrolyte and sediment in low (5–10%) concentration (Figure 9). Two electrodes are also immersed into this suspension, one inside, the other outside of the aperture tube. If an electric field is applied to the electrolyte a current will flow across the aperture. When a sediment grain is caught up in this current it changes the impedance as it passes through the aperture by replacing a volume of electrolyte equal to its own immersed volume. This is then detected as, e.g., a voltage pulse by the instrument. Each voltage pulse above background noise will be registered as a grain, while the height of that pulse, which is proportional to the replaced volume of electrolyte, will be converted into grain size (Beckman Coulter, Inc., 2011, www.beckmancoulter.com). The Coulter Counter "assumes" that grains pass through the aperture one at a time. However, this is not always so. This so-called coincidence reduces the observed number of particles and increases the observed average particle size [*Wynn and Hounslow*, 1997], since in these instances the voltage pulse will be proportional to the combined volume of two or more grains. The instrument does correct for coincidence, but it most probably cannot perfectly account for all such errors. The question is what percentage of all grains in the distribution is artificially generated? While a few such additional grains at the finer end of the distribution would not cause much of a difference in the sortable-silt index, they can potentially introduce a more significant error, if they happen to increase the number of the largest grains in the distribution. In contrast, coincidence is less of a problem if we use differential-number-based statistics.

6. Conclusions

The traditionally used sortable-silt index ($\overline{SS}$) is an arithmetic average computed from the differential volume or mass distribution of grains within a sample; where the weights $\left(\text{i.e., } \frac{V_i}{V} \text{ or } \frac{m_i}{m}\right)$ of the individual size

bins become increasingly disproportionate, with respect to the actual number of grains within those size bins, toward the coarse end of the size range. This does not only increase the absolute value of the apparent "mean size" within the 10–63 μm terrigenous silt fraction, but it may also affect the apparent pattern of relative changes in the coarseness of the sortable-silt fraction along the core. In addition, it makes the sortable-silt index more prone to biases due to random fluctuations in the number percent of the coarsest grains within the samples.

Sortable-silt mean grain diameter ($\bar{d}_{SS}$), on the other hand, better approximates the actual physical size of the average grain within the 10–63 μm terrigenous silt fraction and likely better describes variations in the actual coarseness of the sortable-silt fraction along the core. Moreover, $\bar{d}_{SS}$ may be a more robust measure of current strength, which is likely also less susceptible to analytical errors than $\overline{SS}$.

In general, the finer the sortable-silt fraction, the larger the impact of small changes in the relative number of the largest grains within that size fraction on $\overline{SS}$. Therefore, our results may have particular significance for overflow deposits, which are generally much finer than the sediments used in this study, and for longer time series stretching back into the last deglaciation, when there was likely a regime change in ocean circulation, with a corresponding shift in the mean coarseness of current-sorted deposits.

If our findings from this specific site have general validity, this would question the standard way of documenting grain-size changes, applied in a large number of already published sortable-silt time series. The raw Coulter Counter output (i.e., the pulse data) is often discarded straight after measurement because it takes up a lot of disc space. Without the pulse data it is no longer possible to verify whether $\bar{d}_{SS}$ values would reflect the same pattern of change in the coarseness of the sortable-silt fraction as the already published $\overline{SS}$ time series. Therefore, we recommend colleagues who use the sortable-silt method in the future (and have access to a Coulter Counter) to keep the pulse data and calculate $\bar{d}_{SS}$ values as well to see how the choice of statistics affects their results.

Acknowledgments

This research was carried out within the framework of the ESF EuroMARC project AMOCINT funded by the Research Council of Norway under the NORKLIMA programme and by the Bjerknes Centre for Climate Research (BCCR). The authors would like to thank I. Nicholas McCave, Dag Inge Blindheim, and Tor Mjell for thoughtful discussions, Yusuke Yokoyama and three anonymous reviewers for their comments that led to an improved manuscript, and Dag Inge Blindheim for laboratory assistance. The complete sortable-silt index and sortable-silt mean grain diameter data set, as presented in Figure 2, will be archived via the PANGAEA information system. The data that Figures 5–7 are based upon will be available on request upon publication.

References

Bianchi, G. G., I. R. Hall, I. N. McCave, and L. Joseph (1999), Measurement of the sortable silt current speed proxy using the Sedigraph 5100 and Coulter Multisizer IIe: Precision and accuracy, *Sedimentology*, *46*(6), 1001–1014.

Coakley, J. P., and J. P. M. Syvitski (1991), SediGraph technique, in *Principles, Methods and Application of Particle Size Analysis*, edited by J. P. M. Syvitski, pp. 129–142, Cambridge Univ. Press, N. Y.

Dade, W. B., A. R. M. Nowell, and P. A. Jumars (1992), Predicting erosion resistance of muds, *Mar. Geol.*, *105*(1–4), 285–297.

Dahlgren, K. I. T., and T. O. Vorren (2003), Sedimentary environment and glacial history during the last 40 ka of the Vøring continental margin, mid-Norway, *Mar. Geol.*, *193*(1–2), 93–127.

Ellison, C. R. W., M. R. Chapman, and I. R. Hall (2006), Surface and deep ocean interactions during the cold climate event 8200 years ago, *Science*, *312*(5782), 1929–1932.

Fohrmann, H., J. O. Backhaus, F. Blaume, and J. Rumohr (1998), Sediments in bottom-arrested gravity plumes: Numerical case studies, *J. Phys. Oceanogr.*, *28*(11), 2250–2274.

Fohrmann, H., et al. (2001), Modern ocean current-controlled sediment transport in the Greenland-Iceland-Norwegian (GIN) Seas, in *The Northern North Atlantic: A Changing Environment*, edited by P. Schäfer et al., pp. 135–154, Springer, Berlin.

Fugate, D. C., and C. T. Friedrichs (2003), Controls on suspended aggregate size in partially mixed estuaries, *Estuarine Coastal Shelf Sci.*, *58*(2), 389–404.

Gross, T. F., and A. J. Williams III (1991), Characterization of deep-sea storms, *Mar. Geol.*, *99*(3–4), 281–301.

Hjøllo, S. S. (1999), *A Comparative Study of the Norwegian Sea Inflow*, Geophys. Inst., Univ. of Bergen, Bergen, Norway.

Holtedahl, H. (1981), Distribution and origin of surface sediments on the Norwegian continental margin between 62°N and 65°N, with some remarks on the Late Quaternary litho- and biostratigraphy, in *The Norwegian Coastal Current*, edited by R. Sætre and M. Mork, pp. 768–793, Univ. of Bergen, Bergen, Norway.

Hoogakker, B. A. A., M. R. Chapman, I. N. McCave, C. Hillaire-Marcel, C. R. W. Ellison, I. R. Hall, and R. J. Telford (2011), *North Atlantic Holocene Sortable Silt Grain Size Data, IGBP PAGES/World Data Cent. for Paleoclimatol. Data Contrib. Ser. 2011-143*, NOAA/NCDC Paleoclimatol. Program, Boulder, Colo.

Hunt, J. R. (1986), Particle aggregate breakup by fluid shear, in *Estuarine Cohesive Sediment Dynamics*, edited by A. J. Mehta, pp. 85–109, Springer, N. Y.

Laberg, J. S., et al. (2005), Cenozoic alongslope processes and sedimentation on the NW European Atlantic margin, *Mar. Pet. Geol.*, *22*(9–10), 1069–1088.

Ledbetter, M. T., and D. A. Johnson (1976), Increased transport of Antarctic bottom water in the vema channel during the last ice age, *Science*, *194*(4267), 837–839.

Mauritzen, C. (1996), Production of dense overflow waters feeding the North Atlantic across the Greenland-Scotland Ridge. Part 1: Evidence for a revised circulation scheme, *Deep Sea Res., Part I*, *43*(6), 769–806.

McCave, I. N. (2007), Chapter one deep-sea sediment deposits and properties controlled by currents, in *Proxies in Late Cenozoic Paleoceanography*, edited by C. Hillaire–Marcel and A. De Vernal, pp. 19–62, Elsevier, N. Y.

McCave, I. N., and I. R. Hall (2006), Size sorting in marine muds: Processes, pitfalls, and prospects for paleoflow-speed proxies, *Geochem. Geophys. Geosyst.*, *7*, Q10N05, doi:10.1029/2006GC001284.

McCave, I. N., and S. A. Swift (1976), A physical model for the rate of deposition of fine-grained sediments in the deep sea, *Geol. Soc. Am. Bull.*, *87*(4), 541–546.

McCave, I. N., and J. P. M. Syvitski (1991), Principles and methods of geological particle size analysis, in *Principles, Methods and Application of Particle Size Analysis*, edited by J. P. M. Syvitski, pp. 3–12, Cambridge Univ. Press, N. Y.

McCave, I. N., B. Manighetti, and S. G. Robinson (1995), Sortable silt and fine sediment size/composition slicing: Parameters for palaeocurrent speed and palaeoceanography, *Paleoceanography*, *10*(3), 593–610.

McCave, I. N., I. R. Hall, and G. G. Bianchi (2006), Laser vs. settling velocity differences in silt grain-size measurements: Estimation of palaeocurrent vigour, *Sedimentology*, *53*(4), 919–928.

Mehta, A. J., and J. W. Lott (1987), Sorting of fine sediment during deposition, in *Coastal Sediments*, edited by N. C. Kraus, pp. 348–362, Am. Soc. of Civ. Eng., N. Y.

Miller, M. C., and P. D. Komar (1977), The development of sediment threshold curves for unusual environments (Mars) and for inadequately studied materials (foram sands), *Sedimentology*, *24*(5), 709–721.

Mork, K. A., and Ø. Skagseth (2010), A quantitative description of the Norwegian Atlantic Current by combining altimetry and hydrography, *Ocean Sci.*, *6*(4), 901–911.

Moros, M., K. Emeis, B. Risebrobakken, I. Snowball, A. Kuijpers, J. McManus, and E. Jansen (2004a), Sea surface temperatures and ice rafting in the Holocene North Atlantic: Climate influences on northern Europe and Greenland, *Quat. Sci. Rev.*, *23*(20–22), 2113–2126.

Moros, M., J. F. McManus, T. Rasmussen, A. Kuijpers, T. Dokken, I. Snowball, T. Nielsen, and E. Jansen (2004b), Quartz content and the quartz-to-plagioclase ratio determined by X-ray diffraction: A proxy for ice rafting in the northern North Atlantic?, *Earth Planet. Sci. Lett.*, 218(3–4), 389–401.

Oehmig, R. (1993), Entrainment of planktonic foraminifera: Effect of bulk density, *Sedimentology*, *40*(5), 869–877.

Orvik, K. A., and P. Niiler (2002), Major pathways of Atlantic water in the northern North Atlantic and Nordic Seas toward Arctic, *Geophys. Res. Lett.*, *29*(19), 1896, doi:10.1029/2002GL015002.

Praetorius, S. K., J. F. McManus, D. W. Oppo, and W. B. Curry (2008), Episodic reductions in bottom-water currents since the last ice age, *Nat. Geosci.*, *1*(7), 449–452.

Rumohr, J., F. Blaume, H. Erlenkeuser, H. Fohrmann, F.-J. Hollender, J. Mienert, and C. Schäfer-Neth (2001), Records and processes of near-bottom sediment transport along the Norwegian-Greenland Sea margins during Holocene and Late Weichselian (Termination I) times, in *The Northern North Atlantic: A Changing Environment*, edited by P. Schäfer et al., pp. 155–178, Springer, Berlin.

Ryan, W. B. F., et al. (2009), Global multi-resolution topography synthesis, *Geochem. Geophys. Geosyst.*, *10*, Q03014, doi:10.1029/2008GC002332.

Self, R. F. L., A. R. M. Nowell, and P. A. Jumars (1989), Factors controlling critical shears for deposition and erosion of individual grains, *Mar. Geol.*, *86*(2–3), 181–199.

Singer, J. K., J. B. Anderson, M. T. Ledbetter, I. N. McCave, K. P. N. Jones, and R. Wright (1988), An assessment of analytical techniques for the size analysis of fine-grained sediments, *J. Sediment. Res.*, *58*(3), 534–543.

Søiland, H., M. D. Prater, and T. Rossby (2008), Rigid topographic control of currents in the Nordic Seas, *Geophys. Res. Lett.*, *35*, L18607, doi:10.1029/2008GL034846.

Stein, R. (1985), Rapid grain-size analyses of clay and silt fraction by Sedigraph 5000D: Comparison with Coulter Counter and Atterberg methods, *J. Sediment. Petrol.*, *55*(4), 590–593.

Syvitski, J. P. M., K. W. G. LeBlanc, and K. W. Asprey (1991), Interlaboratory, interinstrument calibration experiment, in *Principles, Methods and Application of Particle Size Analysis*, edited by J. P. M. Syvitski, pp. 174–194, Cambridge Univ. Press, Cambridge, U. K.

Tegzes, A. D., E. Jansen, and R. J. Telford (2014), The role of the northward-directed (sub)surface limb of the Atlantic Meridional Overturning Circulation during the 8.2 ka event, *Clim. Past*, *10*(5), 1887–1904.

Thornalley, D. J. R., M. Blaschek, F. J. Davies, S. Praetorius, D. W. Oppo, J. F. McManus, I. R. Hall, H. Kleiven, H. Renssen, and I. N. McCave (2013), Long-term variations in Iceland-Scotland overflow strength during the Holocene, *Clim. Past*, *9*(5), 2073–2084.

Voet, G., D. Quadfasel, K. A. Mork, and H. Søiland (2010), The mid-depth circulation of the Nordic Seas derived from profiling float observations, *Tellus, Ser. A*, *62*(4), 1–14.

Wynn, E. J. W., and M. J. Hounslow (1997), Coincidence correction for electrical-zone (Coulter-counter) particle size analysers, *Powder Technol.*, *93*(2), 163–175.